Nanoscale

PAPER

View Article Online
View Journal | View Issue

Cite this: *Nanoscale*, 2026, **18**, 8731

Single-particle ICP-MS characterization of magnetoliposomes: toward measurement of the number distribution of encapsulated magnetic nanoparticles

Linda Ayouni-Derouiche, *[a] Jules Mistral, [b] Ece Ates, [b] Marie Boutry,[a] Nadia Baskali-Bouregaa, [a] Laurent David, [b] Sabri Derouiche[a] and Catherine Ladavière *[b]

Magnetoliposomes (MLs) are very pertinent candidates for biomedical applications. They can be used as drug delivery vectors and magnetic resonance imaging (MRI) contrast agents. Their characterization in terms of size and size distribution by dynamic light scattering (DLS), surface charge by electrophoretic light scattering, and morphology by (cryo)-transmission electron microscopy (TEM) is well documented in the literature. However, no study on the distribution of the number of encapsulated magnetic nanoparticles (NPs) per ML has been reported thus far, despite its importance in the design of efficient MLs for targeted applications. The work presented herein reveals that this information could be obtained by employing a relatively innovative technique, *i.e.* single-particle inductively coupled plasma-mass spectrometry (spICP-MS). This required the development of an orderly calculation methodology and a mathematical treatment of raw data detailed herein, and validated on four different concentrations of MLs. The results for the number of encapsulated magnetic NPs per ML show satisfactory agreement among the concentrations, confirming the suitability of this technique for characterization of MLs.

Received 25th July 2025,
Accepted 26th February 2026

DOI: 10.1039/d5nr03155a

rsc.li/nanoscale

Introduction

Magnetoliposomes (MLs) are liposomes embedding magnetic nanoparticles (NPs). Firstly described by De Cuyper and Joniau in 1988,[1] these objects have attracted increasing interest over the last decades in drug delivery applications. Indeed, the association of a lipid carrier with NPs presenting excellent magnetic properties leads to a multifunctional platform that can control the delivery of encapsulated bioactive agents to a region of interest, which can be monitored by MRI. Although the prospects for clinical applications are still far, significant progress have been made in recent years, both in the development of MLs, and in the demonstration of a controlled delivery of bioactive agents under a pulsed[2–5] or static[6] magnetic field.

Generally, two categories of MLs have been developed and distinguished according to the location of the magnetic NPs in the lipid self-assembly. Indeed, these NPs can be inserted inside the lipid membrane or encapsulated within the vesicular aqueous cavity.[7] This location is conditioned by the hydrophilic or hydrophobic nature of the surface coating of magnetic NPs. In most cases, these NPs are superparamagnetic iron oxide NPs with a surface stabilized by electrostatic or/and steric interactions. The ones with a hydrophilic surface coating are preferentially located in the aqueous cavity of MLs, whereas those with a hydrophobic coating are positioned in their lipid membrane. The location, and consequently the nature of the surface coating of magnetic NPs, is often selected according to the intended application.[7] MLs as contrast agents for MRI often encapsulate magnetic NPs in their aqueous cavity.[8,9] Conversely, the lipid membrane is generally preferred for applications in the delivery of hydrophilic bioactive agents in order to avoid possible interactions between the magnetic NPs and the encapsulated bioactive agents.[10,11]

Concerning the encapsulation process, achieving homogeneity in magnetic NPs inside liposomes is a decisive challenge in obtaining MLs with optimal magnetic properties. Nevertheless, to the best of our knowledge, this aspect has never been reported in the literature. Instead, MLs are often examined by dynamic light scattering (DLS) to determine their size and size distribution and by electrophoretic light scattering to measure their surface charge. Transmission electron

[a]*Université Claude Bernard Lyon 1, CNRS, ISA, UMR5280, 5 rue de la Doua, F-69100 Cedex, Villeurbanne, France. E-mail: linda.ayouni-derouiche@isa-lyon.fr*
[b]*Université Claude Bernard Lyon 1, INSA Lyon, Université Jean Monnet, CNRS UMR 5223, Ingénierie des Matériaux Polymères, F-69622 Cedex, Villeurbanne, France. E-mail: catherine.ladaviere@univ-lyon1.fr*

microscopy (TEM), sometimes under cryogenic conditions, often complete these analyses by providing information on the morphology of these objects.[12–14] Besides these techniques, a few studies used inductively coupled plasma-mass spectrometry (ICP-MS)[15] and atomic absorption spectroscopy[16] to determine the total concentration of iron (Fe) in the analyzed samples.

With the aim of determining the distribution in the number of magnetic NPs per ML, the innovative analytical single-particle ICP-MS (spICP-MS) technique[17,18] was used in this work. It combines the benefits of an element-specific atomic spectrometry technique (such as ICP-MS), with those of a particle-counting technique (measurements performed on a particle-by-particle basis). Thus, this technique can provide information on size, particulate and ionic concentrations, without being combined with other techniques. Established by Degueldre *et al.*[19] in 2003, it has been increasingly used up thus far, and its development for the analysis of NPs with different chemical natures began in 2010 (SI1). The principle of spICP-MS is based on that of ICP-MS, a technique introduced in the mid-1980s. In "sp" mode, the sample follows the same path as in ICP-MS, with the difference that the sample in "sp" mode is a very diluted NP suspension with a concentration of the order of a hundred ng L^{-1}, and that the apparatus operates in "time-resolved analysis" process with a high acquisition frequency. This leads to the detection of signal pulses, where each one corresponds to an ion cloud formed by only one NP based on the assumption that the NP suspension dilution and the acquisition frequency are well adapted. The NP size is correlated with the intensity of the signal pulse and the particulate concentration is given by the number of pulses, whereas the ionic concentration is determined by the intensity of the baseline signal. This spICP-MS technique has already been used for the analysis of different types of NPs (*e.g.*, titanium dioxide,[20] gold,[21] and silver[22] NPs, see SI1), which requires specific methodology optimization due to the specificities of each type of NPs.

Concerning iron oxide NPs, due to their increasing valorization in the biomedical field, their characterization by spICP-MS has become necessary. However, one of the major problems in the analysis of these NPs employing this technique is the interference from the $^{40}Ar^{16}O^{+}$ polyatomic ion (when argon is used as the plasma gas) on the most abundant iron isotope, the ^{56}Fe isotope (both have the same m/z ratio of 56). Many efforts have been made to overcome this interference without compromising the sensitivity of the analysis.[23] We previously showed that this issue was resolved by decreasing the forward power, and by using high-energy helium as the collision gas.[24] Based on this optimization of the analytical conditions, magnetic NPs inside magnetoliposomes have been studied herein.

The main aim of the work presented herein is to show that it is possible to determine the number distribution of magnetic NPs encapsulated in MLs employing the spICP-MS technique. This determination involved the development of a calculation methodology and mathematical treatment of the raw data, which are presented in the first part of this article. To examine their robustness, the analyses of four different concentrations of the same purified ML suspension are detailed and discussed in the second part.

Experimental section

Materials

Iron(II) chloride tetrahydrate ($FeCl_2{\cdot}4H_2O$, purity ≥99%), iron (III) chloride hexahydrate ($FeCl_3{\cdot}6H_2O$, purity ≥ 99%), ammonium hydroxide (28%–30%), and citric acid (99%) were obtained from Sigma-Aldrich (France). Hydrochloric acid (HCl, 37%), chloroform, and sodium chloride were supplied by Carlo Erba Reagents (France). Ultrapure water was obtained from the Aguettant laboratory (France) for the synthesis of magnetic NPs and magnetoliposomes. Zwitterionic 1,2-dipalmitoyl-*sn-glycero*-3-phosphocholine (DPPC, $C_{40}H_{80}NO_8P$) lipid, cationic 1,2-dipalmitoyl-3-trimethylammonium propane (DPTAP, $C_{38}H_{76}NO_4Cl$) lipid, and anionic 1,2-dipalmitoyl-*sn-glycero*-3-phosphoethanolamine-*N*-[methoxy(polyethyleneglycol)-5000] (DPPE-PEG5000, $C_{265}H_{531}NO_{123}P$) polymer–lipid conjugate were purchased from Avanti Polar Lipids Inc. (USA). All lipids were used without further purification. The dialysis membrane with a molecular weight cut-off (MWCO) of 3.5 kDa used at the end of the magnetic NP synthesis was purchased from Spectrum Laboratories (USA). A magnetoliposome extrusion kit and polycarbonate membrane with pore diameters of 200 nm and 400 nm, respectively, were obtained from Avanti Polar Lipids Inc. (USA). D-Tube Dialyzers Maxi® was obtained from Millipore (France). Sodium silicotungstate used for TEM observations was obtained from Sigma Chemical Co. (USA).

Synthesis of magnetic NPs surface-stabilized with citric acid

Superparamagnetic iron oxide NPs of magnetite (Fe_3O_4), hereafter named "magnetic NPs", were synthesized using a co-precipitation method, as previously described.[25] A solution of 50 mL deionized water and 310 μL hydrochloric acid (HCl) was stirred at 60 rpm in a round-bottom flask. $FeCl_3{\cdot}6H_2O$ and $FeCl_2{\cdot}4H_2O$ iron salts were added in a 2 : 1 molar stoichiometric ratio (0.905 g and 0.333 g, respectively), along with an additional 50 mL of distilled water. The stirring rate was then increased to 80–90 rpm. The mixture was subjected to argon gas during the entire procedure. The flask was placed in an oil bath at 60 °C for 1 h. Subsequently, the stirring rate was increased to 170–180 rpm, and 15 mL of ammonium hydroxide was added dropwise, resulting in the immediate appearance of a black precipitate, indicating the successful synthesis of Fe_3O_4 magnetic NPs. After 30 minutes, the temperature was increased to 90 °C, and 0.967 g of citric acid (CA) was added, with stirring continuing for an additional 90 minutes. Following this, heating and stirring were ceased, and the CA-coated Fe_3O_4 magnetic NPs (Fe_3O_4:CA) were isolated using magnetic decantation. The supernatant was discarded, and 5 mL of deionized water was added to redisperse the magnetic

NP suspension, which was then transferred into a dialysis membrane (MWCO of 3.5 kDa) and dialyzed against deionized water for 24 hours (6 different baths, dialysate/bath volume ratio = 1/200) to reach neutral pH and remove any unabsorbed CA molecules. Subsequently, 1 mL of the Fe_3O_4 magnetic NP suspension was withdrawn and dried to evaluate the mass concentration of magnetic NPs in the aqueous suspension.

Synthesis of MLs densely loaded with magnetic NPs

MLs were prepared using the Bangham film hydration technique,[26] following a protocol described elsewere.[27] Briefly, predetermined quantities of DPPC, DPPE-PEG 5000, and DPTAP lipids (6.60 mg, 2.87 mg, and 0.32 mg, respectively) were dissolved in chloroform. The solvent was evaporated at 60 °C under vacuum to form a uniform thin lipid film, which was subsequently hydrated (20 minutes, 60 °C) under rotating stirring using 1 mL of an ultrasonicated Fe_3O_4 magnetic NP suspension at a concentration of 30 mg mL^{-1}. This resulted in an ML suspension with a lipid concentration of 10 mM and a DPPC/DPTAP/DPPE-PEG5000 molar ratio of 90/5/5. Then, the ML suspension was extruded at 70 °C through two consecutive polycarbonate membranes with pore sizes of 400 nm and 200 nm, respectively, passing 11 times through each membrane. This procedure yielded a final size-monodisperse suspension of MLs.

Removal of unencapsulated magnetic NPs by salt-induced aggregation from ML suspensions

A given volume of 5 M NaCl solution was added to an ML suspension to achieve a final NaCl concentration of 0.45 M. The mixture was then centrifuged for 3 minutes at 4000*g* and 25 °C. The pellet containing unencapsulated magnetic NPs was removed, and the supernatant was subjected to overnight dialysis against deionized water (MWCO 12–14 kDa, dialyzate-to-bath volume ratio of 1/200) to remove any remaining salts from the ML suspension.

Removal of empty liposomes by magnetic chromatography from ML suspensions

The ML suspension previously purified *via* salt-induced aggregation was passed through a MACS® column (MS column, Miltenyi Biotec, Germany) positioned within a permanent magnet (Mini Macs Separator, Miltenyi Biotec). Empty liposomes without magnetic NPs were immediately eluted, whereas MLs containing encapsulated magnetic NPs were magnetically retained in the column. The immobilized MLs were then rinsed with 5 mL of deionized water before being eluted with 1 mL of deionized water by removing the column from the magnetic field. This elution step was precisely controlled, as it determined the final concentration of the purified ML suspension. The water elution process was repeated twice.

Characterization of ML suspensions by dynamic light scattering (DLS)

The average hydrodynamic diameters of the MLs were measured at 25 °C in deionized water using a Zetasizer Nano ZS (Malvern Instruments, UK). The laser used was a helium–neon type, operating at a wavelength of 633 nm, with a scattering angle of 173°. Magnetic NPs and unpurified ML suspensions were diluted 100-fold in ultrapure water prior to the analysis, while liposomes and purified ML suspensions (following either the salt-induced aggregation step alone or both salt-induced aggregation and magnetic chromatography steps) were diluted 20-fold in ultrapure water. The refractive index and viscosity of ultrapure water at 25 °C were set to 1.33 and 0.8904 cP, respectively. Typically, three independent measurements were performed for the determination of average hydrodynamic diameter.

Characterization of ML suspensions by cryo-transmission electron microscopy (TEM)

A small volume (~3.5 μL) of ML suspension was placed on a copper grid coated with a Lacey carbon film (EMS). The excess liquid was promptly blotted with filter paper, leaving a thin film of the sample spread across the grid. The grid was then rapidly vitrified by plunging it into liquid ethane, cooled by liquid nitrogen, using a Thermo Fisher Scientific Vitrobot. Once vitrified, the grid was transferred into liquid nitrogen and loaded into a cryo-holder (Fischione Instruments model 2550) maintained at −174 °C. The holder was quickly inserted into the vacuum column of the transmission electron microscope. Observations were performed at CTμ (Villeurbanne, France) using a JEOL 1400 Flash microscope, equipped with a Gatan Rio16 camera, in low-dose mode at an accelerating voltage of 120 kV.

Quantification of iron and phosphorous elements in ML suspensions by inductively coupled plasma mass spectrometry (ICP-MS)

Standard solutions of iron and phosphorus (1 g L^{-1}) were diluted to produce calibration concentrations of 0, 5, 10, 20, 50, and 100 μg L^{-1}, all prepared in 2% vol. Suprapur HNO_3. The ML suspensions were digested using a microwave digestion system (UltraWAVE, Milestone, Italy), a process referred to as "mineralization" in this study. In this procedure, 50 μL of each ML suspension was placed into a Pyrex® digestion tube, followed by the addition of 3 mL of 65 vol% Suprapur HNO_3. The mixture was digested according to a temperature program that involved heating to 220 °C for 20 min, followed by a 20 min hold at 220 °C. After digestion, the resulting solutions were diluted to 50 mL with deionized water, and further diluted to match the calibration curve concentrations. The total analysis was conducted using internal calibration with yttrium as the internal standard. Measurements were performed using an Agilent 8800 and Agilent 7900 ICP-MS (Agilent Technologies), equipped with a MicroMist nebulizer, a Scott-type spray chamber, and a torch with a 2.5 mm internal diameter injector. To address interferences during the measurement of $^{56}Fe^+$ and $^{31}P^+$, a collision reaction cell (CRC) was used. The high-energy helium (HEHe) mode was employed for iron, and oxygen was used as the reaction gas for phosphorus, in combination with an MS/MS in tandem mode. Note

that it was checked that the mineralization step was total on an unpurified ML sample with a known iron concentration.

Characterization of ML suspensions by spICP-MS

Analysis of the ML suspensions was carried out using an Agilent 7900 ICP-MS system (Agilent Technologies, Japan), equipped with a single-particle analysis module of the Agilent MassHunter® workstation software. The introduction system consisted of a MicroMist nebulizer, a Scott-type spray chamber, and a torch with an injector of 2.5 mm internal diameter. The instrument was fitted with an octopole collision reaction cell (CRC) and a quadrupole mass analyzer positioned downstream to detect the mass-to-charge ratios.

The Agilent 7900 ICP-MS system, with a plasma power of 1200 W, uses helium as the collision gas. Optimized gas flow was determined using the ramp cell tool in the MassHunter software at a flow rate from 0 to 8 mL min^{-1} in increments of 0.5 mL min^{-1} while monitoring the background and iron signals. The optimal helium flow was identified to be equal to 4.8 mL min^{-1} to maximize the signal-to-background (S/B) ratio.

The detector was an electron multiplier operating at high-frequency data acquisition rates, with a dwell time of 0.1 ms herein. The lowest dwell times led to better definitions of signals, where a dwell time of 0.1 ms was the lowest value achievable with the Agilent 7900 ICP-MS system. Operational parameters included an argon plasma gas flow of 15.5 mL min^{-1}, nebulizer gas flow of 1.0 mL min^{-1}, spray chamber cooling at 2 °C, and a peristaltic pump speed of 0.1 rps. The flow rate of sample was 0.346 mL min^{-1}, with an optimal sample depth of 6.5 mm. The accuracy of this flow rate was verified by weighing a quantity of water analyzed over a given time.

Daily lens tuning was performed prior to each batch analysis using a tuning solution containing Co, Mg, Li, Y, Tl, and Ce at a concentration of 1 μg L^{-1}. A performance report, based on 10 measurements, was generated to check the sensitivity, relative standard deviation, oxide ratio ($^{140}Ce^{16}O^{+}/^{140}Ce^{+}$), and doubly charged ions ($^{140}Ce^{2+}/^{140}Ce^{+}$). The pulse/analog (P/A) factor was calibrated with a 150 μg L^{-1} multi-element solution.

For spICP-MS analysis, the iron sensitivity factor was determined using an ionic blank and a 10 μg L^{-1} iron ionic standard. The transport efficiency (TE) was calculated by the software using the size-based method with a 1 μg L^{-1} gold ionic standard and a 60 nm gold NP suspension as the calibration standard.[28] Obtaining an accurate transport efficiency is crucial for reliable results, which requires well-characterized NP suspensions. In this case, a 60 nm Au NP suspension from Sigma Aldrich was analyzed using spICP-MS, with a 50 nm NP standard from nanoComposix for comparison. The measured size (59.4 ± 0.5 nm) was consistent with the specifications provided by the supplier. The iron concentrations in the ML suspensions were determined without the "peak integration" mode in the Agilent MassHunter® workstation software.

Results and discussion

As mentioned, the determination by spICP-MS of the number distribution of magnetic NPs encapsulated in MLs has never been reported in the literature to the best of our knowledge. Thus, optimization of the spICP-MS technical conditions for analyzing magnetic NP suspensions was required. This was previously published in a technical note,[29] as well as the development of a specific calculation methodology and mathematical treatment for the ML suspensions, as presented below. Indeed, the analysis of ML suspensions by spICP-MS, during which each signal pulse corresponds to each NP reaching the detector, is more complicated than that of "simple" NP suspensions. For the ML suspensions, one ML leads to several signal pulses on the detector, which represent several encapsulated magnetic NPs in an ML. Consequently, the crossing delay of one ML in front of the detector has to be determined and linked to its encapsulated magnetic NP number. Moreover, this number of magnetic NPs has to be calculated from raw data comprising not only signals of magnetic NPs but also background ones. Thus, a methodical mathematical selection of signal pulses corresponding to only magnetic NPs has to be performed from a raw analysis data file, which is composed of up to 600 000 lines. As a result of this, the exploitation of spICP-MS data files needs to be carefully carried out by developing a rational calculation methodology and a mathematical program, as described in the first part of this article.

Secondly, the robustness of the developed calculation methodology and mathematical treatment was checked by analyzing four different concentrations (corresponding to iron concentrations of 69, 138, 276, and 553 ppt measured by ICP-MS) of the same purified ML suspension. These results in terms of average magnetic NP number per ML and the distribution of this number are compared and discussed in the second part of this article.

Description of the calculation methodology and mathematical treatment of spICP-MS raw data

A method for processing the spICP-MS raw measurement data was developed to obtain the number distribution of encapsulated magnetic NPs per ML and its average. It includes a calculation methodology and mathematical treatment constituted of seven different steps, as summarized and presented below.

Step 1. Determination of threshold between background and magnetic NP signals. The threshold defines the limit between the background and magnetic NP signals. Its determination is crucial, and was the subject of a dedicated technical note.[29] Briefly, the threshold position was obtained by using the RStudio® software, and an iterative method well described by Pace *et al.*[28] The signal data are averaged and the standard deviation (σ) is calculated. All the data points above the mean plus 3σ are removed, and this process is repeated until there are no more data points 3σ above the final mean. Thereby, the resulting mean is considered as the threshold. It is assumed that the background data points have a normal distribution. In this work, an additional preliminary step, as described in the

technical note, was introduced, which consists of removing the most frequent blank values to improve the threshold reliability and reduce false positives.

Step 2. Selection of signal pulse intensities above the threshold. All the signal pulse intensities above the pre-determined threshold are selected and retained in the final measurement file (the signal pulse intensities below this threshold are eliminated from this file).

Step 3. Transformation of each signal pulse intensity in a mass of magnetic NPs. The mass of magnetic NPs for each signal pulse intensity, m_{NP}, was determined by using the following equation (eqn (1)):

$$m_{NP} = \left[\frac{(I - I_{bg}) \cdot IE \cdot TE}{\left(\frac{a \cdot 60}{Dt \cdot Q \cdot 1000}\right)}\right] f \quad (1)$$

where m_{NP}: magnetic NP mass, I: pulse intensity value (cps), I_{bg}: background intensity (cps), IE: ionisation efficiency (which is considered as equal to 1), TE: transport efficiency, a: sensitivity (cps ppb^{-1}), Dt: dwell time (ms), Q: sample flow (mL min^{-1}), and f: mass fraction of the element in the magnetic NP ($f = (3 \times 56 + 4 \times 16)/(3 \times 56) = 1.38$).

Step 4. Determination of crossing delay of one ML in front of the detector. To determine the crossing delay of one ML in front of the detector, the total number of MLs crossing the detector during the total acquisition time in the delay analysis (60 s) was first calculated. This total number of MLs was calculated based on the measurement of the phosphorous concentration of the considered sample by ICP-MS. This phosphorous concentration is transformed into the total number of lipids in the analyzed suspension. The total number of lipids is divided by the number of lipids composing one ML (determined by dividing the total area of one spherical ML, with a DLS average diameter of 120 nm and PDI of 0.09, by the area of one lipid head), giving the total number of MLs. Secondly, the crossing delay of one ML in front of the detector is obtained by dividing the total acquisition time delay of the analysis (60 s) by the total number of MLs corrected for TE (3.2%). This crossing delay of one ML was found to be 48, 24, 12, and 6 ms for suspensions with iron concentrations of 69, 138, 276, and 553 ppt, respectively. Note that Toska *et al.*,[24] who determined the iron mass distribution in suspensions of hybrid silica methacrylate colloids (not in MLs), did not determine this crossing delay for one colloid. They used a suspension dilution that they considered to be sufficient to detect only one colloid in front of the detector during their dwell time of 0.1 ms.

Step 5. Determination of the mass of magnetic NPs during the crossing delay of one ML in front of the detector. To determine the mass of magnetic NPs during the crossing delay of one ML in front of the detector, the Python® software was used to gather the masses detected during the previously determined crossing delay of one ML and to add them to one mass corresponding to the mass of all the magnetic NPs encapsulated in one ML.

Step 6. Determination of magnetic NP number during the crossing delay of one ML in front of the detector. To obtain the number of magnetic NPs during the crossing delay of one ML in front of the detector, each mass calculated in step 5 (contained in one ML) was divided by the mass of one magnetic NP, $m_{one\ NP}$, obtained from the following equation (eqn (2)):

$$m_{one\ NP} = \frac{d^3 \cdot \rho \cdot \pi}{6} \quad (2)$$

where $m_{one\ NP}$: mass of one magnetic NP, d: magnetic NP diameter, and ρ: volumetric mass, considering that these magnetic NPs are spherical, with a diameter of 10 nm, as previously observed and measured by TEM.[25]

Step 7. Determination of average and distribution of magnetic NP number per ML. Finally, the average and the distribution of magnetic NP number per ML were represented by a log–normal distribution (see equation in SI2).

Exploitation of spICP-MS raw data by using the developed calculation methodology and mathematical treatment

Based on the previously developed calculation methodology and mathematical treatment, the raw data of four different ML concentrations (see SI3) were processed to obtain the number distribution of encapsulated magnetic NPs per ML and its average. These four concentrations were obtained by preparing an initial ML suspension with an iron concentration of 0.069 g L^{-1} (69 × 10^6 ppt) and diluting it in water by factors of 10^6, 5 × 10^5, 2.5 × 10^5, and 1.5 × 10^5, yielding final iron concentrations of 69, 138, 276, and 553 ppt, respectively. The iron concentrations of these four suspensions (69, 155, 247, and 520 ppt), measured using the Agilent MassHunter® spICP-MS workstation software, and by integrating all the signal pulses of the magnetic NPs, were found to be in agreement with the expected iron concentrations. This reveals the validity of steps 1 and 2 of the calculation methodology that we developed before.

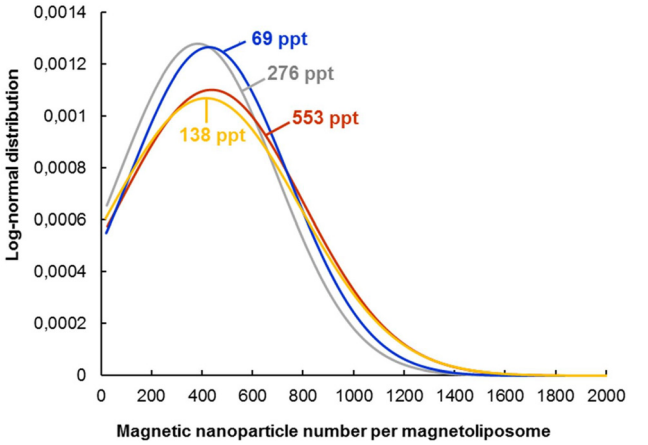

Fig. 1 Log–normal distributions of the encapsulated magnetic NP number per magnetoliposome (ML) measured by spICP-MS as a function of the iron concentration (ppt) measured by ICP-MS.

For information purposes, step 5 allows the calculation of the total number of MLs detected during the total acquisition time (60 s) for each analyzed concentration. This ML number corresponds to number of lines obtained from the Python® software. As expected, these numbers increased with the iron concentration (69, 138, 276, and 553 ppt), and were found to be 883, 1788, 3288, and 6811 MLs, respectively.

Concerning step 7, it gives the number of encapsulated magnetic NPs per ML. This number can be represented in a log–normal distribution as a function of the iron concentration (Fig. 1).

Table 1 Averages and distributions (standard deviations) calculated from log–normal distributions of the magnetic NP number per magnetoliposome (ML) measured by spICP-MS as a function of the iron concentration measured by ICP-MS

Iron concentration	Average	Standard deviation
69 ppt	428	315
138 ppt	416	373
276 ppt	384	312
553 ppt	438	362
Average	**417**	**341**
Standard deviation	**23**	**32**
Variation%	**6**	**9**

Fig. 1 reveals similar distributions in the encapsulated magnetic NP number per magnetoliposome regardless of the iron concentration. All these distributions are large, ranging from 1 to 1 500, and are centered between 350 and 450. Table 1 shows the data from the analysis of these log–normal distribution. According to it, the average magnetic NP number per ML of four concentrations is 417 with a standard deviation of 23, representing a satisfactory analytic variation of 6%. The distribution width (*i.e.*, the standard deviation of the log–normal distribution, Table 1) also displays a satisfactory variation (9%) for the four concentrations since the average value is 341 ± 32. As a result, these variations (6% and 9%) reveal a correct repeatability of analyses, as well as a validation of the calculation methodology and mathematical treatment for these four independent suspensions.

Concerning the distribution of encapsulated magnetic NP number per ML (*i.e.*, 341 ± 32, Table 1), it has been found to be very broad as this encapsulated magnetic NP number ranges from approximately 75 to 760 (for 68% of data around the mean, 417 ± 341). This very broad number distribution can be correlated with the cryo-TEM observations of these samples, showing MLs with very different loadings of magnetic NPs (Fig. 2). It is unfortunately impossible to calculate the average number of magnetic NPs per ML directly from the

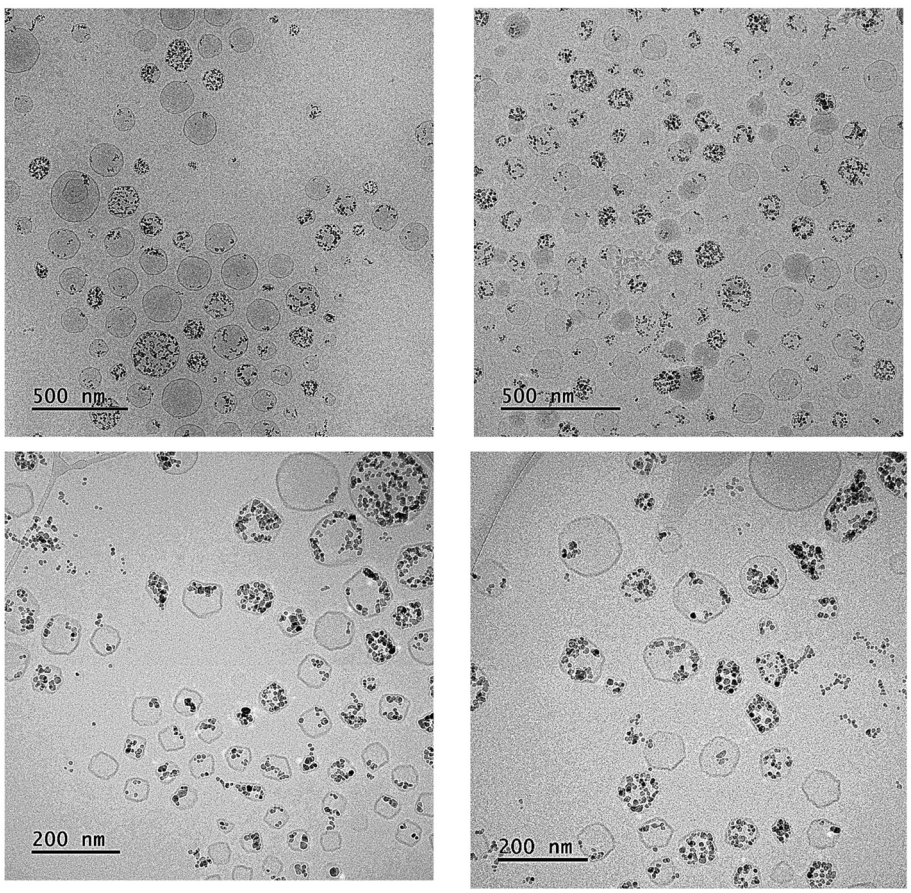

Fig. 2 Cryo-TEM of MLs showing the broad number distribution of the encapsulated magnetic NP number per magnetoliposome (ML).

cryo-TEM images because these 2D images are projections of 3D objects, with overlays of magnetic NPs at different z positions. Nevertheless, cryo-TEM provides complementary information that supports the broad distribution in NP encapsulation revealed by spICP-MS.

Finally, for comparison, a standard ICP-MS analysis was applied to determine the average number of magnetic NPs per ML of the same initial ML batch. This technique presents two main drawbacks *versus* spICP-MS in the context that it does not give access to the number distribution and it requires a mineralization step. The calculation of the average number of magnetic NPs per ML by ICP-MS was based on the assayed phosphorous and iron concentrations, mass density of Fe_3O_4, average sizes of the magnetic NPs and MLs (10 and 120 nm, respectively), lipid concentration and the surface of a lipid head. This calculation, with the details given in SI4, leads to an average of 315 ± 37 magnetic NPs per ML (on 3 replicates) compared to 417 ± 23 determined by spICP-MS. This comparison very promisingly reveals the same order of magnitude of this number average. The value of 315 ± 37 by ICP-MS is close of the top of the spICP-MS curves in Fig. 1. Note that the difference between both techniques is relatively small given the very wide distribution of encapsulated magnetic NP number per ML (*i.e.*, ±341, Table 1), as well as the different technical constraints specific to each of these techniques (supplementary mineralization step and total digestion required in ICP-MS, necessary calculation of the crossing delay of one ML in front of the detector, and extreme dilution in spICP-MS).

Conclusion

In conclusion, this work demonstrates that spICP-MS can be very useful to determine not only the average number of encapsulated magnetic NPs per ML, but also its distribution in the suspension. This requires a calculation methodology and mathematical treatment of the raw data, which were detailed in seven steps herein and validated on four different concentrations of purified ML suspensions. To the best of our knowledge, this notion of number dispersion is obtained herein for the first time while this information can be very important to increase the homogeneity of magnetic NP loading of MLs by optimizing the different stages of the ML elaboration. Moreover, it can improve the understanding of the link between the design of MLs and their efficiency in biomedical applications.

Author contributions

Linda Ayouni-Derouiche: funding acquisition, conceptualization, methodology, supervision, investigation, writing – review & editing, Jules Mistral: investigation, writing – original draft, writing – review & editing, Ece Ates: investigation, Marie Boutry: investigation, Nadia Baskali-Bouregaa: writing – review & editing, Laurent David: funding acquisition, writing – review & editing, Sabri Derouiche: software, Catherine Ladavière: funding acquisition, conceptualization, methodology, supervision, writing – original draft, writing – review & editing.

Conflicts of interest

There are no conflicts to declare.

Data availability

Data are available, upon request, from the authors.

Supplementary information (SI): SI1. Evolution of the number of articles on the spICP-MS technique since 2010, and main types of NPs studied by this technique. SI2. Equation of log–normal distribution. SI3. Representation of the spICP-MS raw data of MLs for four iron concentrations in ppt. SI4. Detailed calculations of the average number of magnetic NPs per ML measured by ICP-MS. See DOI: https://doi.org/10.1039/d5nr03155a.

Acknowledgements

This work was partially funded by a grant from Institut de Chimie de Lyon (ICL). The authors gratefully acknowledge Pierre Alcouffe for the cryo-TEM images and the "CTμ" (Centre Technologique des Microstructures de l'Université Lyon 1) platform for the access to cryo-TEM.

References

1 M. De Cuyper and M. Joniau, Magnetoliposomes: Formation and structural characterization, *Eur. Biophys. J.*, 1988, **15**(5), 311–319.
2 G. Podaru, S. Ogden, A. Baxter, T. Shrestha, S. Ren, P. Thapa, R. K. Dani, H. Wang, M. T. Basel, P. Prakash, S. H. Bossmann and V. Chikan, Pulsed Magnetic Field Induced Fast Drug Release from Magneto Liposomes via Ultrasound Generation, *J. Phys. Chem. B*, 2014, **118**(40), 11715–11722.
3 S. Nappini, S. Fogli, B. Castroflorio, M. Bonini, F. Baldelli Bombelli and P. Baglioni, Magnetic field responsive drug release from magnetoliposomes in biological fluids, *J. Mater. Chem. B*, 2016, **4**(4), 716–725.
4 D. Mertz, O. Sandre and S. Bégin-Colin, Drug releasing nanoplatforms activated by alternating magnetic fields, *Biochim. Biophys. Acta, Gen. Subj.*, 2017, **1861**(6), 1617–1641.
5 M. N. Zharkov, M. V. Gerasimov, D. B. Trushina, D. N. Khmelenin, E. V. Gromova, D. E. Yakobson and M. A. Pyataev, Two types of magnetite-containing liposomes for magnetocontrolled drug release, *J. Phys.: Conf. Ser.*, 2019, **1389**(1), 012070.

6 J. Mistral, N. Milhau, D. Pin, O. Chapet, P. Nunes De Oliveira, A. Serghei, G. Sudre, C. Ladavière and L. David, *Small*, 2026, e11451.
7 C. A. Monnier, D. Burnand, B. Rothen-Rutishauser, M. Lattuada and A. Petri-Fink, Magnetoliposomes: opportunities and challenges, *Eur. J. Nanomed.*, 2014, **6**(4), 201–215.
8 B. Garnier, S. Tan, S. Miraux, E. Bled and A. R. Brisson, Optimized synthesis of 100 nm diameter magnetoliposomes with high content of maghemite particles and high MRI effect: Synthesis of 100 nm magnetoliposomes with high iron content, *Contrast Media Mol. Imaging*, 2012, **7**(2), 231–239.
9 G. Béalle, R. Di Corato, J. Kolosnjaj-Tabi, V. Dupuis, O. Clément, F. Gazeau, C. Wilhelm and C. Ménager, Ultra Magnetic Liposomes for MR Imaging, Targeting, and Hyperthermia, *Langmuir*, 2012, **28**(32), 11834–11842.
10 I. Waheed, A. Ali, H. Tabassum, N. Khatoon, W.-F. Lai and X. Zhou, Lipid-based nanoparticles as drug delivery carriers for cancer therapy, *Front. Oncol.*, 2024, **14**, 1296091.
11 M. E. Fortes Brollo, A. Domínguez-Bajo, A. Tabero, V. Domínguez-Arca, V. Gisbert, G. Prieto, C. Johansson, R. Garcia, A. Villanueva, M. C. Serrano and M. d. P. Morales, Combined Magnetoliposome Formation and Drug Loading in One Step for Efficient Alternating Current-Magnetic Field Remote-Controlled Drug Release, *ACS Appl. Mater. Interfaces*, 2020, **12**(4), 4295–4307.
12 W. I. Choi, A. Sahu, F. R. Wurm and S.-M. Jo, Magnetoliposomes with size controllable insertion of magnetic nanoparticles for efficient targeting of cancer cells, *RSC Adv.*, 2019, **9**(26), 15053–15060.
13 O. Bixner and E. Reimhult, Controlled magnetosomes: Embedding of magnetic nanoparticles into membranes of monodisperse lipid vesicles, *J. Colloid Interface Sci.*, 2016, **466**, 62–71.
14 A. Hardiansyah, F. Destyorini, Y. Irmawati, M.-C. Yang, C.-M. Liu, E. R. Chaldun, M.-C. Yung and T. Y. Liu, Characterizations of doxorubicin-loaded PEGylated magnetic liposomes for cancer cells therapy, *J. Polym. Res.*, 2019, **26**(12), 282.
15 N. Kostevšek, C. C. L. Cheung, I. Serša, M. E. Kreft, I. Monaco, M. Comes Franchini, J. Vidmar and W. T. Al-Jamal, Magneto-Liposomes as MRI Contrast Agents: A Systematic Study of Different Liposomal Formulations, *Nanomaterials*, 2020, **10**(5), 889.
16 C. Moloney, T. R. Chaudhuri, J. A. Spernyak, R. M. Straubinger and D. F. Brougham, Long-circulating magnetoliposomes as surrogates for assessing pancreatic tumour permeability and nanoparticle deposition, *Acta Biomater.*, 2023, **158**, 611–624.
17 C. Davison, D. Beste, M. Bailey and M. Felipe-Sotelo, Expanding the boundaries of atomic spectroscopy at the single-cell lev el: critical review of SP-ICP-MS, LIBS and LA-ICP-MS advances for the elemental analysis of tissues and single cells, *Anal. Bioanal. Chem.*, 2023, **415**(28), 6931–6950.
18 K. Flores, R. S. Turley, C. Valdes, Y. Ye, J. Cantu, J. A. Hernandez-Viezcas, J. G. Parsons and J. L. Gardea-Torresdey, Environmental applications and recent innovations in single particle i nductively coupled plasma mass spectrometry (SP-ICP-MS), *Appl. Spectrosc. Rev.*, 2021, **56**(1), 1–26.
19 C. Degueldre and P. Y. Favarger, Colloid analysis by single particle inductively coupled plasma-mass spectroscopy: a feasibility study, *Colloids Surf., A*, 2003, **217**(1), 137–142.
20 M. Hadioui, G. Knapp, A. Azimzada, I. Jreije, L. Frechette-Viens and K. J. Wilkinson, Lowering the Size Detection Limits of Ag and TiO_2 Nanopart icles by Single Particle ICP-MS, *Anal. Chem.*, 2019, **91**(20), 13275–13284.
21 A. R. Montoro Bustos, E. J. Petersen, A. Possolo and M. R. Winchester, Interlaboratory Comparison of Single Particle ICP-MS S ize Measurements of NIST Gold Nanoparticle Reference Materials, *Anal. Chem.*, 2015, **87**(17), 8809–8817.
22 D. M. Mitrano, E. K. Lesher, A. Bednar, J. Monserud, C. P. Higgins and J. F. Ranville, Detecting nanoparticulate silver using single–particle inductively cou pled plasma–mass spectrometry, *Environ. Toxicol. Chem.*, 2012, **31**(1), 115–121.
23 A. Rua-Ibarz, E. Bolea-Fernandez, G. Pozo, X. Dominguez-Benetton, F. Vanhaecke and K. Tirez, Characterization of iron oxide nanoparticles by means of single-partic le ICP-mass spectrometry (SP-ICP-MS) – chemical versus physical resolution to overcome spectral overlap, *J. Anal. At. Spectrom.*, 2020, **35**(9), 2023–2032.
24 A. Toska, D. Foix, A. Bousquet, N.-H. Yin, C. Pécheyran and J. Allouche, Iron quantification at the sub femtogram level in magnetite hybrid silica methacrylate core–shell nanocomposite particles by sp-ICP-MS, *J. Anal. At. Spectrom.*, 2024, **39**(6), 1439–1443.
25 J. Mistral, K. Tse Ve Koon, L. Fernando Cotica, G. Sanguino Dias, I. Aparecido Santos, P. Alcouffe, N. Milhau, D. Pin, O. Chapet, A. Serghei, G. Sudre, C. Ladavière, P. Nunes De Oliveira and L. David, Chitosan-Coated Superparamagnetic Fe_3O_4 Nanoparticles for Magnetic Resonance Imaging, Magnetic Hyperthermia, and Drug Delivery, *ACS Appl. Nano Mater.*, 2024, **7**(7), 7097–7110.
26 A. D. Bangham, M. M. Standish and J. C. Watkins, Diffusion of univalent ions across the lamellae of swollen phospholipids, *J. Mol. Biol.*, 1965, **13**(1), 238–252.
27 J. Mistral, E. Ates, N. Milhau, D. Pin, P. Alcouffe, O. Chapet, G. Sudre, L. Ayouni-Derouiche, L. David and C. Ladavière, *Colloids Surf., A*, 2026, **729**, 138919.
28 H. E. Pace, N. J. Rogers, C. Jarolimek, V. A. Coleman, C. P. Higgins and J. F. Ranville, Determining Transport Efficiency for the Purpose of Counting and Sizing Nanoparticles via Single Particle Inductively Coupled Plasma Mass Spectrometry, *Anal. Chem.*, 2011, **83**(24), 9361–9369.
29 M. Boutry, J. Mistral, P. Oliveira, N. Baskali-Bouregaa, F. Bessueille-Barbier, N. Gilon, C. Ladavière and L. Ayouni-Derouiche, Development of a methodology for analyzing nanometer-sized iron oxide by the single particle ICP-MS technique, *J. Anal. At. Spectrom.*, 2024, **39**(7), 1726–1735.

